Supporting information for:

Intercluster Reactions Resulting in Silver-Rich Trimetallic Nanoclusters

Esma Khatun, Papri Chakraborty, Betsy Rachel Jacob, Ganesan Paramasivam, Mohammad Bodiuzzaman, Wakeel Ahmed Dar and Thalappil Pradeep*

Department of Chemistry, DST Unit of Nanoscience (DST UNS) and Thematic Unit of Excellence (TUE)

Indian Institute of Technology Madras

Chennai, 600 036, India

E-mail: pradeep@iitm.ac.in

Table of Contents

List of figures	Description	Page number
S1	UV-vis absorption spectra and ESI MS of Ag_{25} and MAg_{24} where 'M' is Ni, Pd or Pt	3-4
S2	XPS spectrum of $NiAg_{28}$ and time-dependent absorption spectra of $NiAg_{24}$, $NiAg_{28}$ and Ag_{29}	4-5
S3	ESI MS of $PdAg_{28}$ measured under low voltage and low gas pressure conditions	5
S4	XPS and SEM/EDS spectra of $PdAg_{28}$	6
S5	UV-vis absorption spectrum and ESI MS of $PtAg_{28}$	7

S6	The collision-induced dissociation mass spectra of $[NiAg_{28}(BDT)_{12}]^{4-}$ and $[PdAg_{28}(BDT)_{12}]^{4-}$	8
S7	Theoretical structures of various isomers of $NiAg_{28}$ and $PdAg_{28}$	9-10
S8	Concentration-dependent ESI MS of the reaction between $PdAg_{28}$ and Au_{25}	11
S9	Theoretical and experimental isotopic distributions of $PdAu_{12}Ag_{16}$	11
S10	Time-dependent UV-vis absorption spectra of intercluster reaction between $PdAg_{28}$ and Au_{25}	12
S11	Theoretical and experimental isotopic distributions of $PtAu_{12}Ag_{16}$	12
S12	Time-dependent ESI MS of intercluster reaction between $PtAg_{28}$ and Au_{25} showing the reaction at Au_{25}	13
S13	Time-dependent UV-vis absorption spectra of intercluster reaction between $PtAg_{28}$ and Au_{25}	13
S14	Time-dependent ESI MS of $NiAg_{28}$ which show the formation of trimetallic $NiAu_xAg_{28-x}$	14
S15	Experimental and theoretical isotopic patterns of $NiAu_{12}Ag_{16}$	14
S16	Concentration-dependent ESI MS of the reaction between Ag_{29} and Au_{25}	15
S17	Time-dependent absorption spectra of the reaction between Ag_{29} and Au_{25} at room temperature	15
S18	Experimental and theoretical isotopic patterns of $Au_{12}Ag_{17}$	16
S19	Time-dependent ESI MS of the reaction between Ag_{29} and Au_{25} at Au_{25} side (higher temperature)	16
S20	Time-dependent UV-vis absorption spectra of the intercluster reaction between Ag_{29} and Au_{25}	17

S21	Three different DFT optimized geometric isomers of $Au_{12}Ag_{17}$ and their energies	17-18

Supporting information 1:

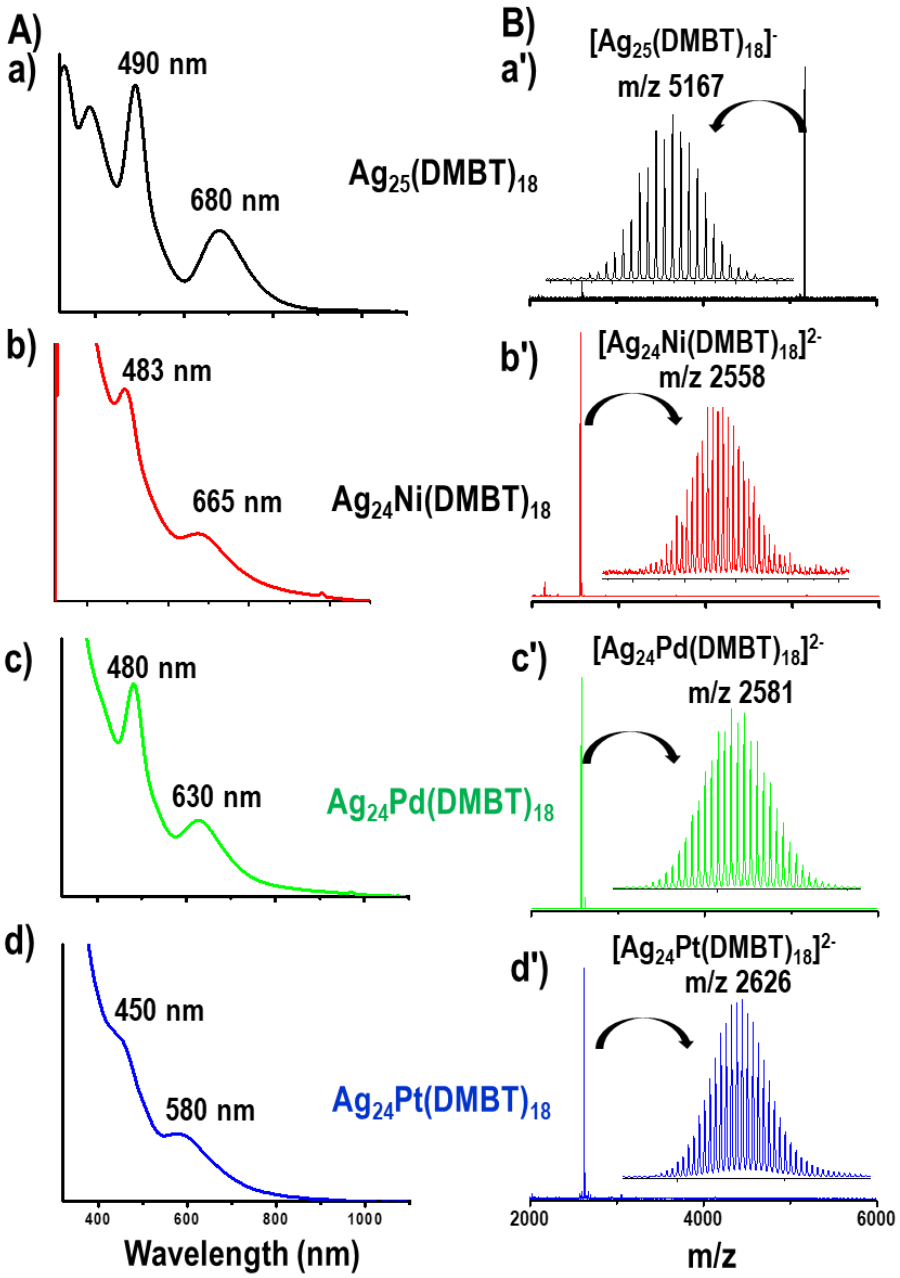

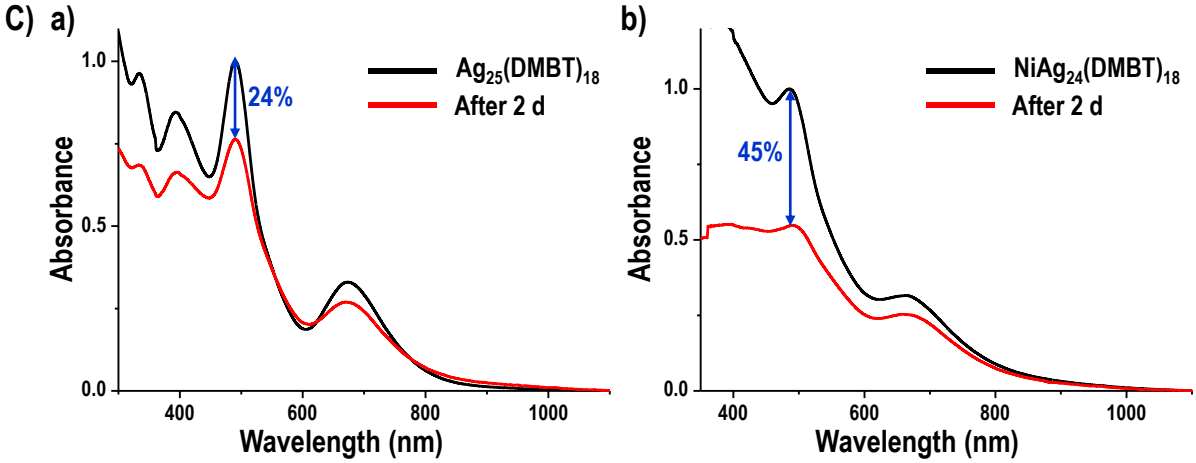

Figure S1. (A) UV-vis absorption spectra and (B) ESI MS of Ag_{25} (panel a/a´) and MAg_{24} where 'M' is Ni, Pd and Pt (panel b/b´, c/c´ and d/d´). Upon doping of Ni, Pd and Pt in Ag_{25}, absorption features show gradual blue-shifts. (C) Time-dependent absorption spectra of (a) Ag_{25} and (b) $NiAg_{24}$ which were kept at room temperature.

Supporting information 2:

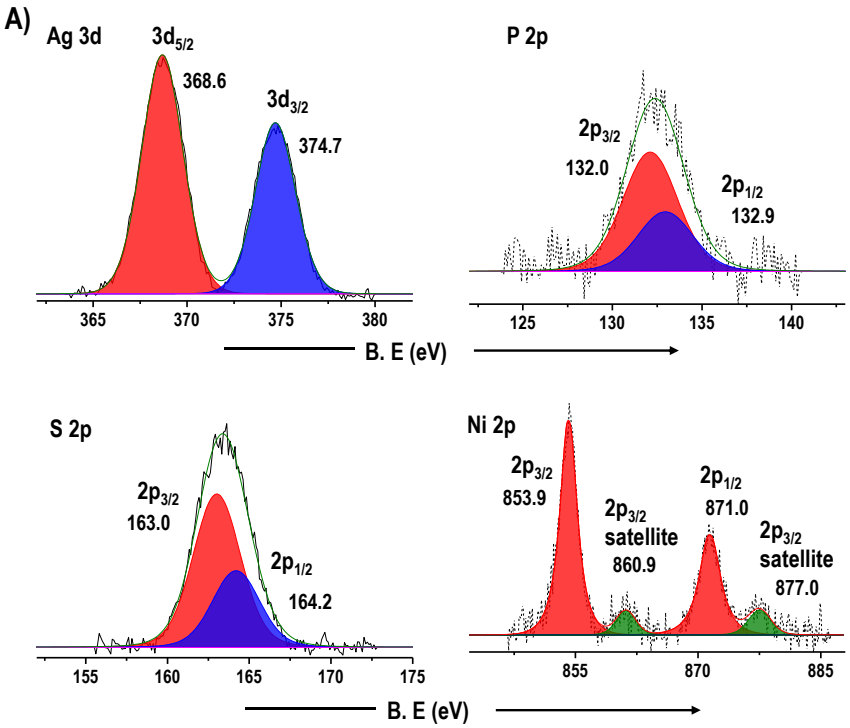

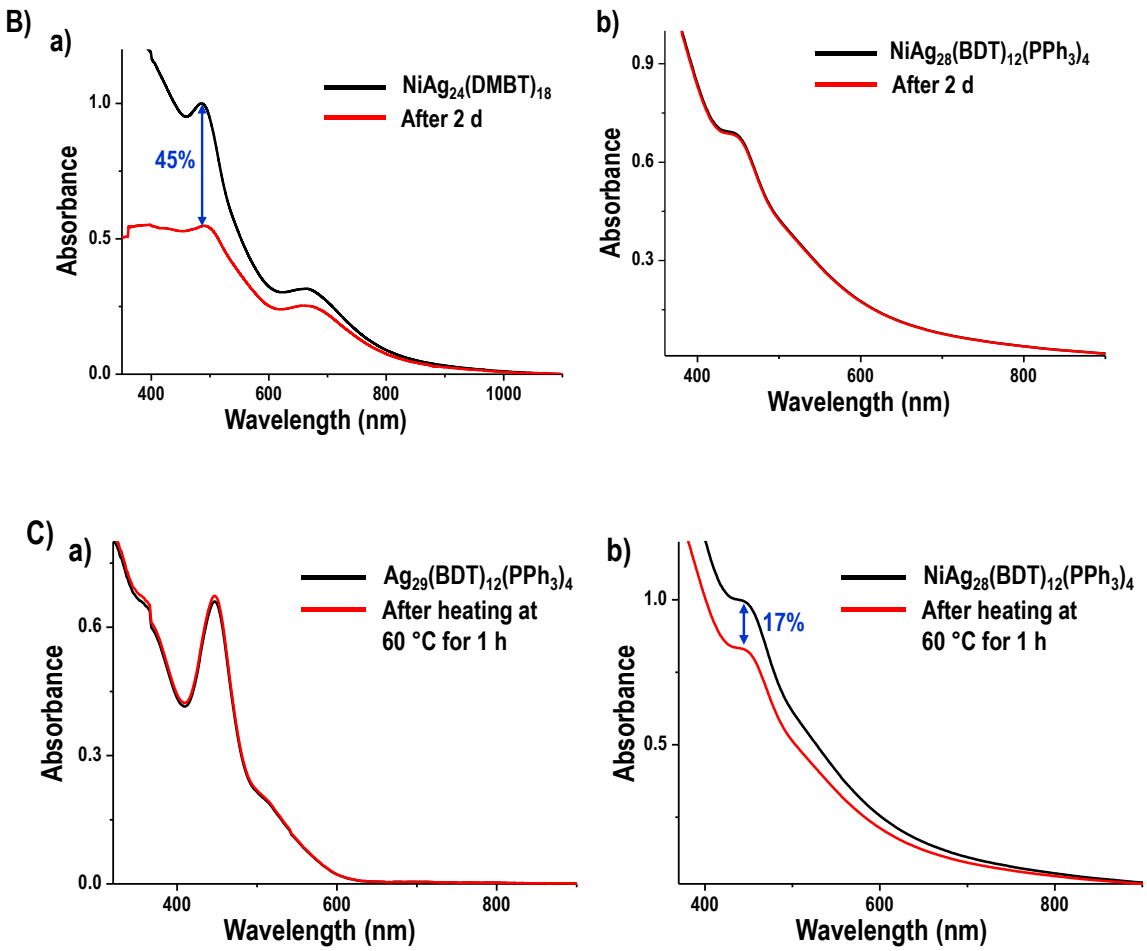

Figure S2. (A) XPS spectrum of $NiAg_{28}$ shows the presence of Ni 2p, Ag 3d, P 2p and S 2p. (B) Time-dependent absorption spectra of (a) $NiAg_{24}$ and (b) $NiAg_{28}$ at room temperature. (C) Time-dependent absorption spectra of (a) Ag_{29} and (b) $NiAg_{28}$ at 60°C temperature.

Supporting information 3:

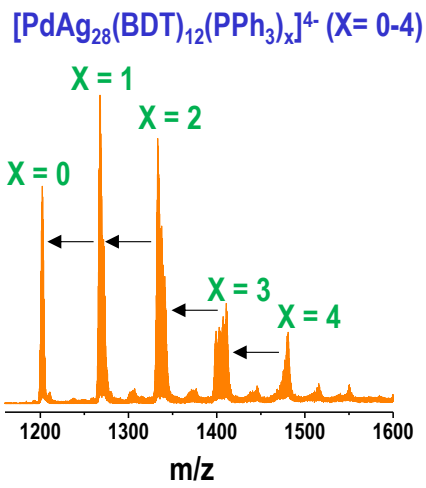

Figure S3. ESI MS of $PdAg_{28}$ measured under low voltage and low gas pressure conditions shows the presence of four PPh_3 ligands.

Supporting information 4:

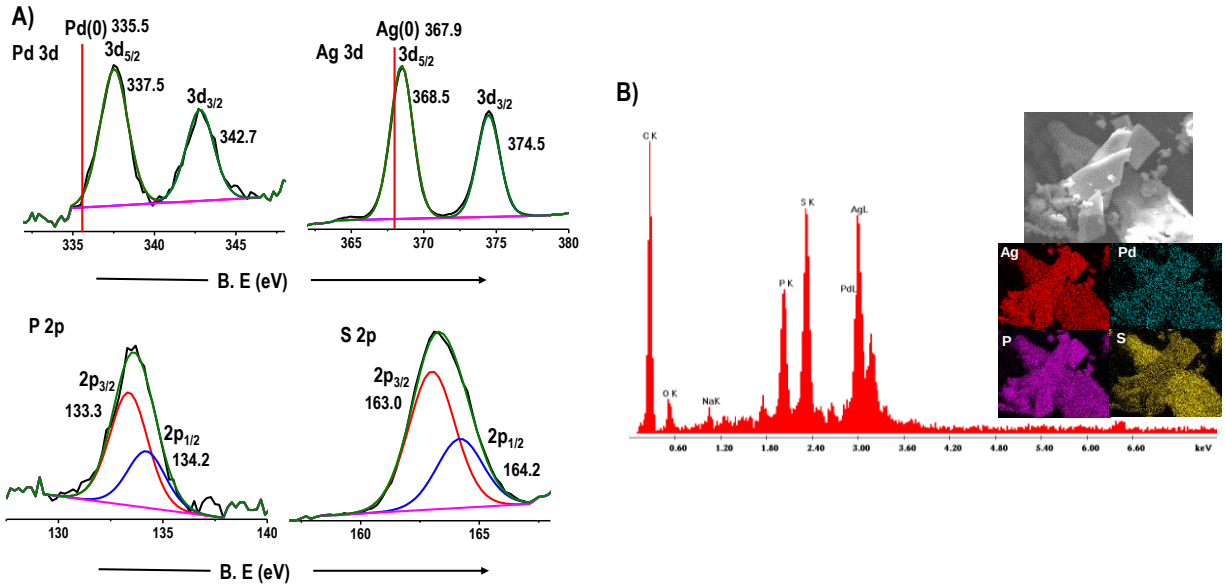

Figure S4. (A) XPS spectrum of $PdAg_{28}$ shows the presence of Pd, Ag, P and S. Pd $3d_{5/2}$ peak arises at 337.5 eV which is higher than that of Pd (0) (335.5 eV) and Ag $3d_{5/2}$ peak arises at 368.5 eV which is also at a higher value than that of Ag (0) (367.9 eV) which manifest a partial charge transfer from Pd to Ag. (B) SEM image of $PdAg_{28}$ and EDS mapping of C, P, S, Ag and Pd.

Supporting information 5:

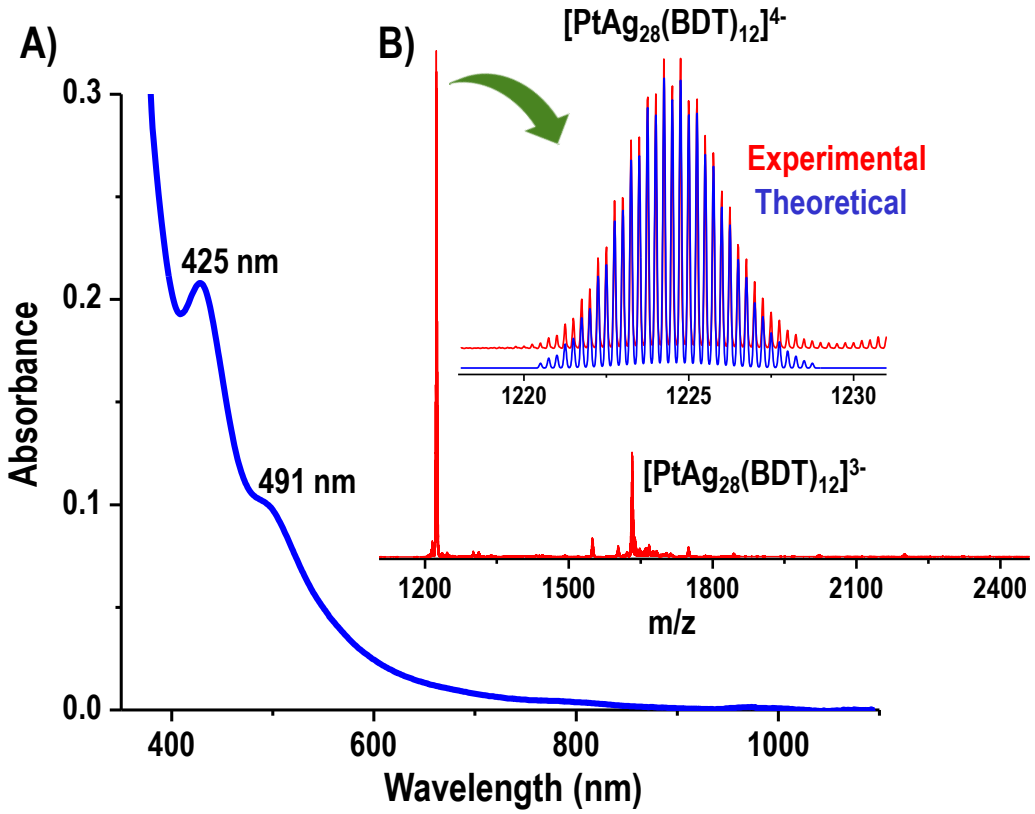

Figure S5. (A) UV-vis absorption spectrum of $PtAg_{28}$ which possesses two prominent features at 425 and 491 nm. The absorption peaks are 22 nm blue-shifted from that of Ag_{29}. (B) ESI MS of $PtAg_{28}$ exhibits two intense peaks at m/z 1224 and 1632 which correspond to $[PtAg_{28}(BDT)_{12}]^{4-}$ and $[PtAg_{28}(BDT)_{12}]^{3-}$, respectively. Theoretical and experimental isotopic distributions of $[PtAg_{28}(BDT)_{12}]^{4-}$ are shown in the inset of (B) which are well fitted.

Supporting information 6:

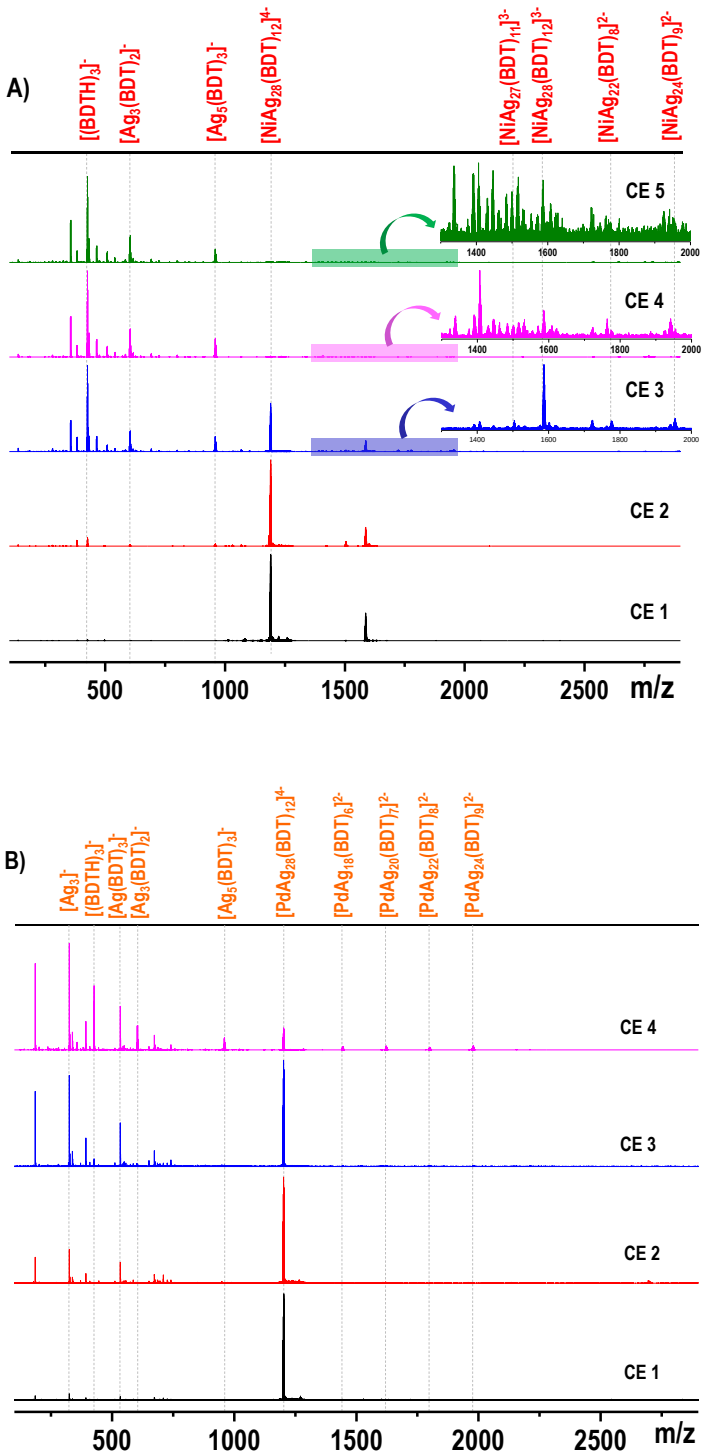

Figure S6. The collision-induced dissociation mass spectra of (A) $[NiAg_{28}(BDT)_{12}]^{4-}$ (m/z 1190) and (B) $[PdAg_{28}(BDT)_{12}]^{4-}$ (m/z 1202).

Supporting information 7:

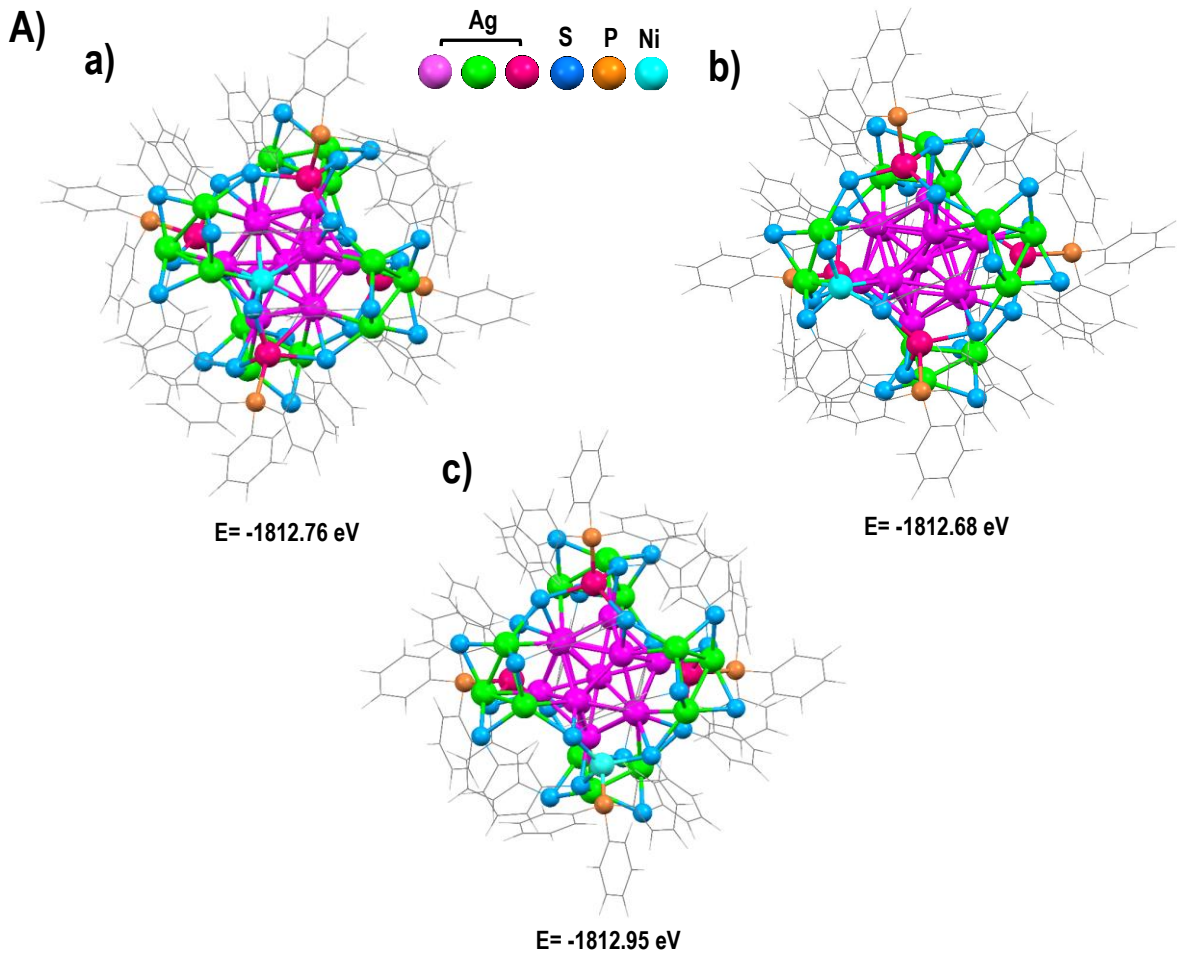

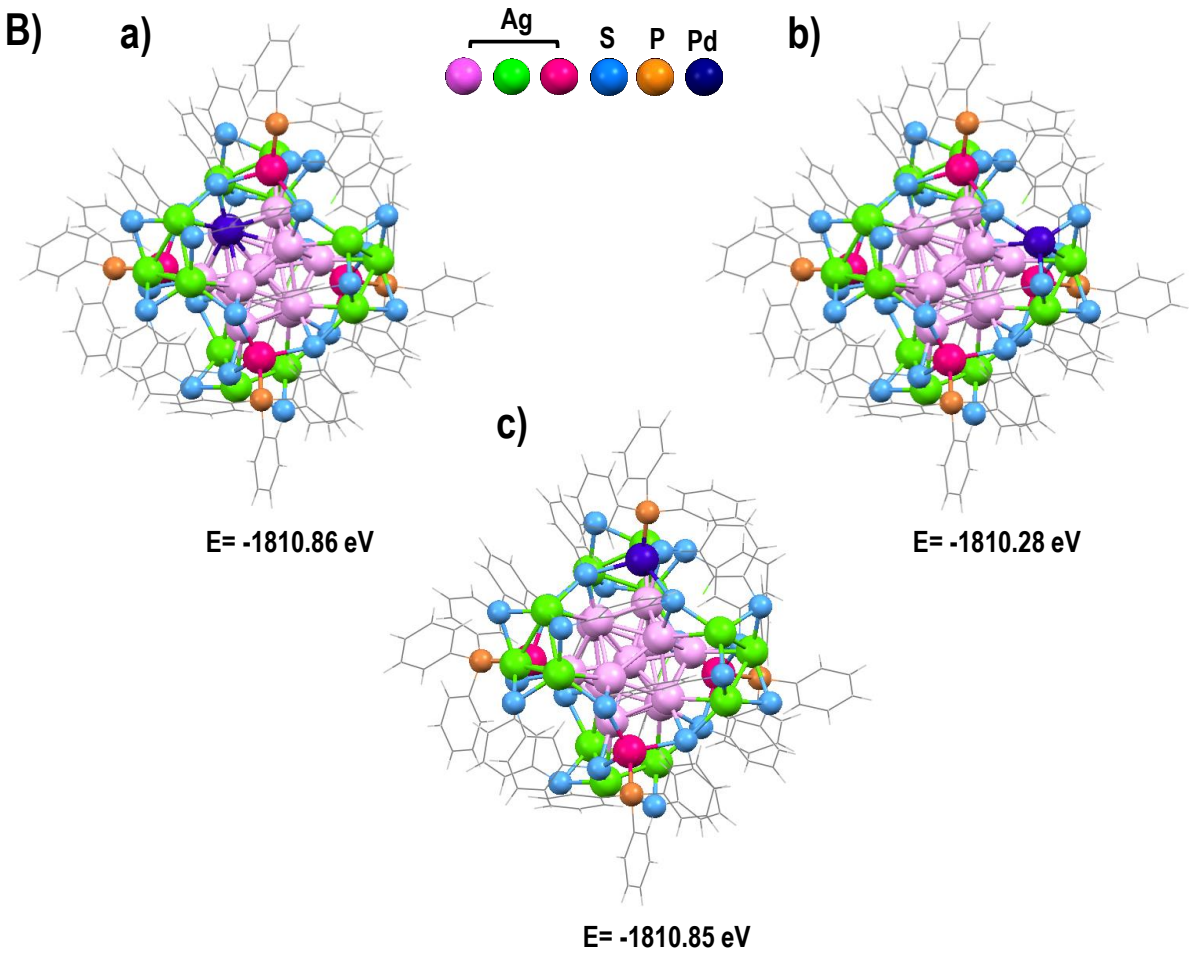

Figure S7. Theoretical structures of different isomers of (A) $NiAg_{28}$ and (B) $PdAg_{28}$. Mainly four isomers of $NiAg_{28}$ and $PdAg_{28}$ were observed and three of them are shown here; (a) Ni/Pd atom is doped in the icosahedral surface, (b) Ni/Pd atom is doped in crown staples and (c) Ni/Pd atom replaces Ag atom which is bonded to PPh_3.

Supporting information 8:

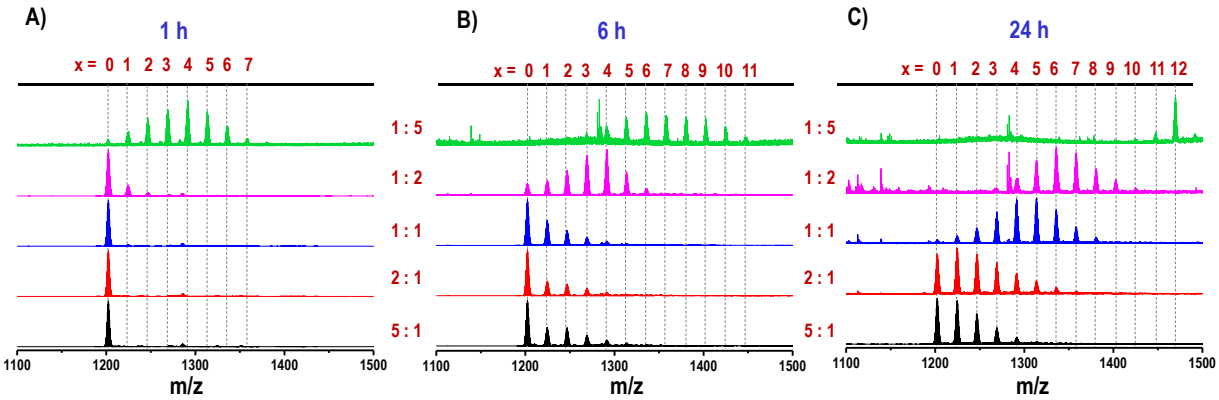

Figure S8. Concentration-dependent ESI MS of the reaction between $PdAg_{28}$ and Au_{25} using 4:1, 2:1, 1:1, 1:2 and 1:5 molar ratios at three different time intervals, (A) 1 h, (B) 6 h and (C) 24 h.

Supporting information 9:

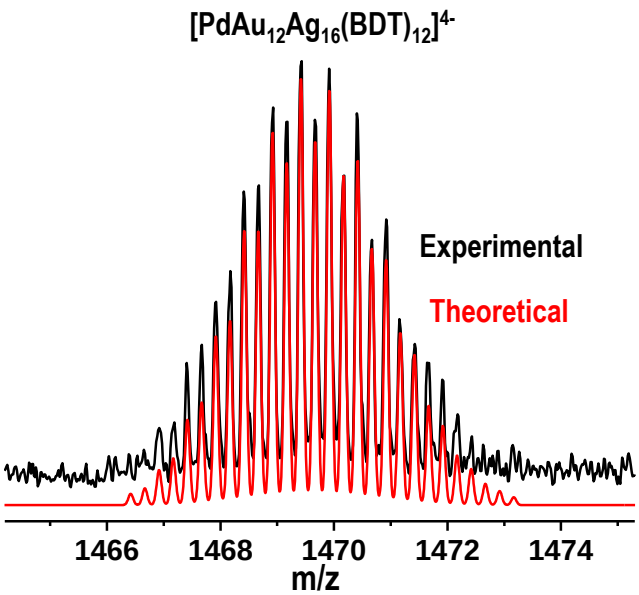

Figure S9. The experimental isotopic distribution (black trace) of $PdAu_{12}Ag_{16}$ which matches exactly with the theoretical one (red trace).

Supporting information 10:

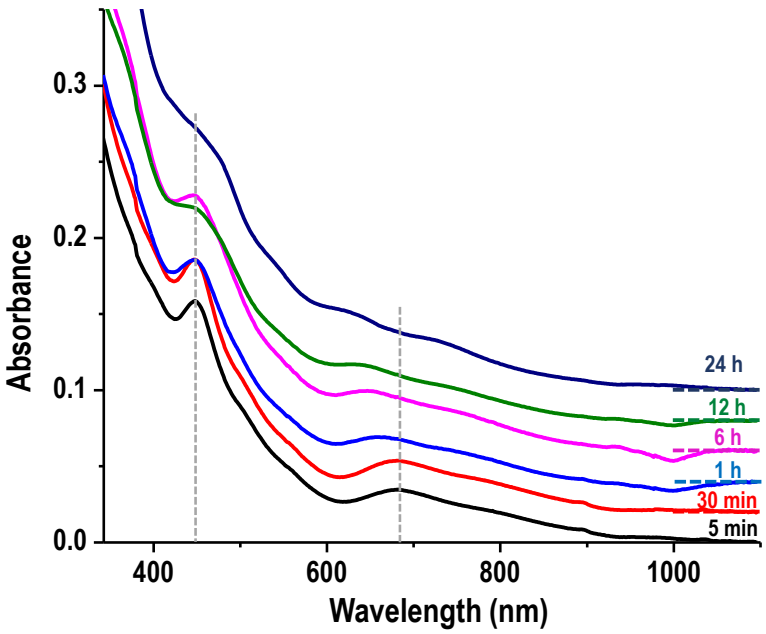

Figure S10. Time-dependent UV-vis absorption spectra of intercluster reaction between $PdAg_{28}$ and Au_{25} using a 1:5 molar ratio.

Supporting information 11:

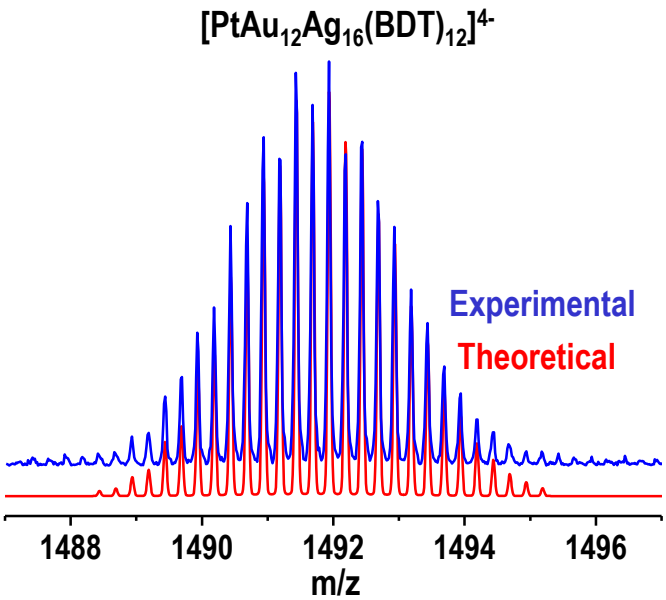

Figure S11. The experimental isotopic distribution (blue trace) of $PtAu_{12}Ag_{16}$ which matches exactly with the theoretical one (red trace).

Supporting information 12:

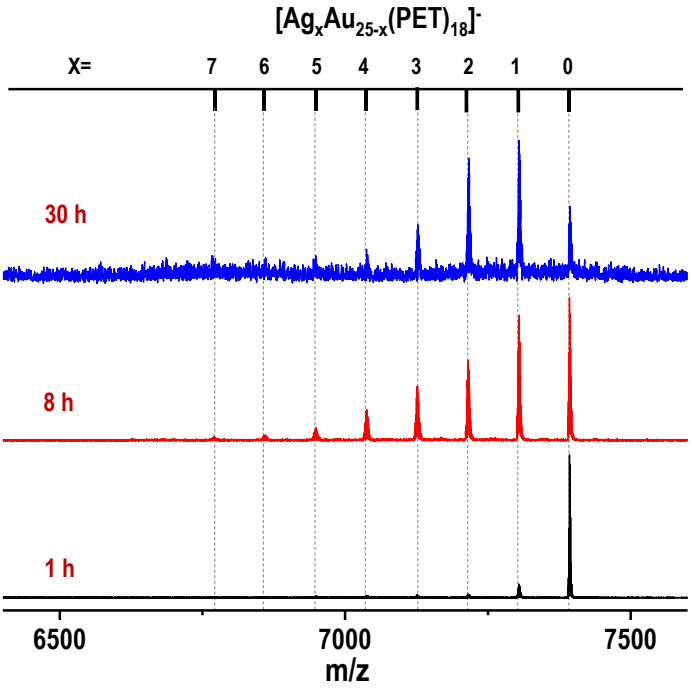

Figure 12. Time-dependent ESI MS of intercluster reaction between $PtAg_{28}$ and Au_{25} (1:5 molar ratio) showing the reaction at Au_{25} side which show formation of Ag_xAu_{25-x} (x= 0-7).

Supporting information 13:

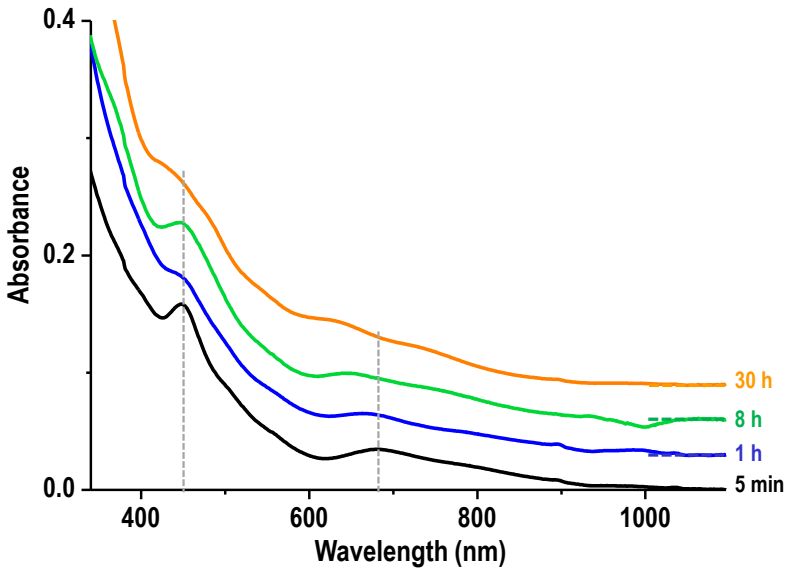

Figure S13. Time-dependent UV-vis absorption spectra of intercluster reaction between $PtAg_{28}$ and Au_{25} using a 1:5 molar ratio.

Supporting information 14:

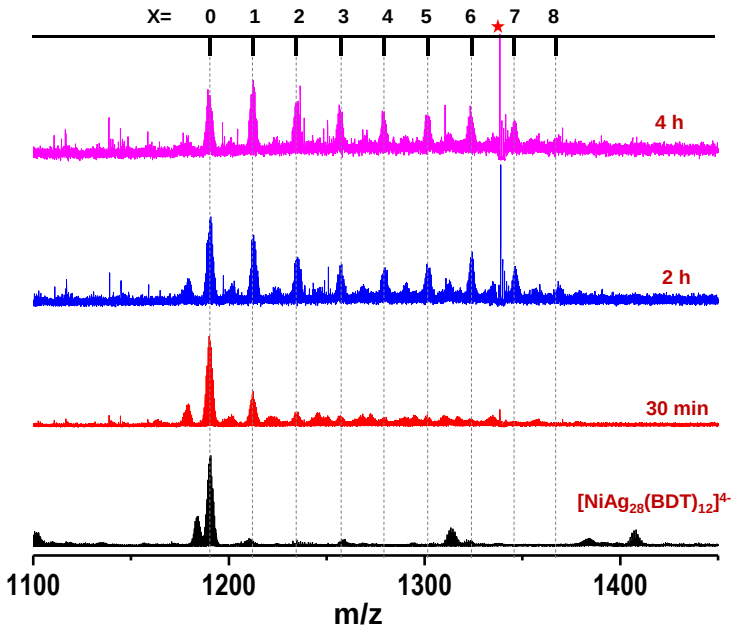

Figure S14. Time-dependent ESI MS of intercluster reaction between $NiAg_{28}$ and Au_{25} using a 1:5 molar ratio which show the formation of trimetallic $NiAu_xAg_{28-x}$.

Supporting information 15:

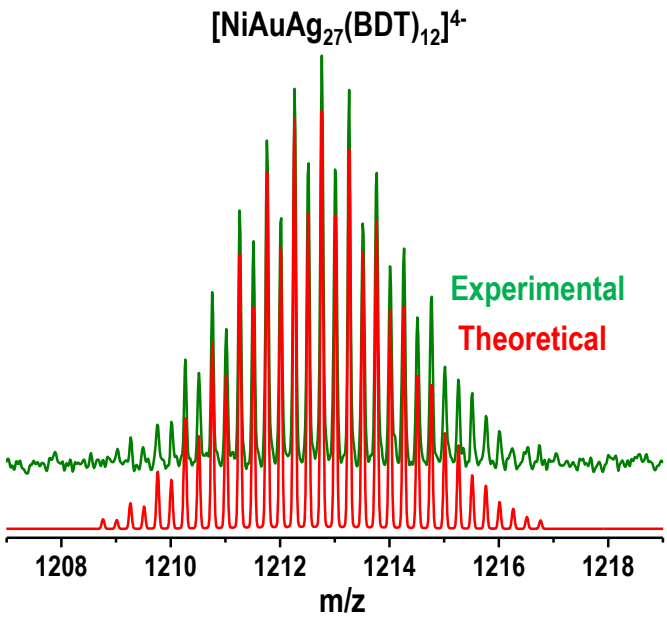

Figure S15. Experimental and theoretical isotopic patterns (green trace) of $NiAuAg_{27}$ (red trace) fit well with each other.

Supporting information 16:

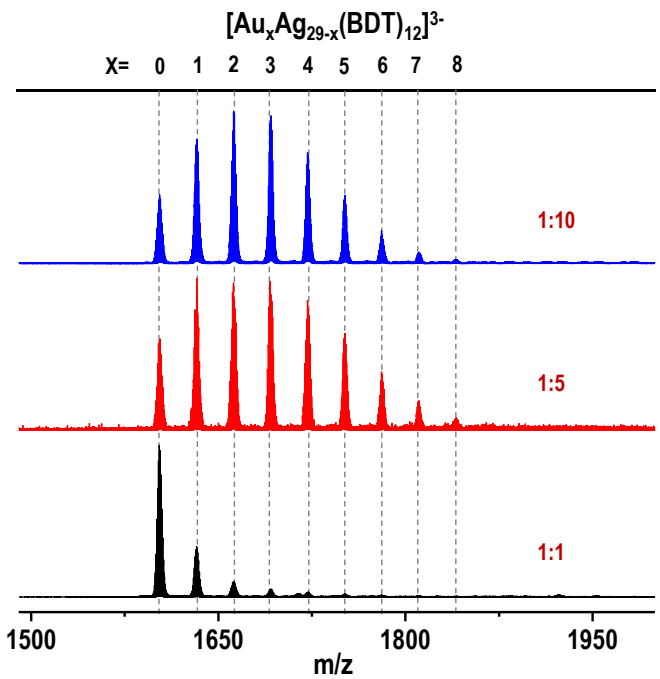

Figure S16. Concentration-dependent ESI MS of the reaction between Ag_{29} and Au_{25} using 1:1, 1:5 and 1:10 molar ratios at 6h which lead to the formation of Au_xAg_{29-x} (x = 1-8).

Supporting information 17:

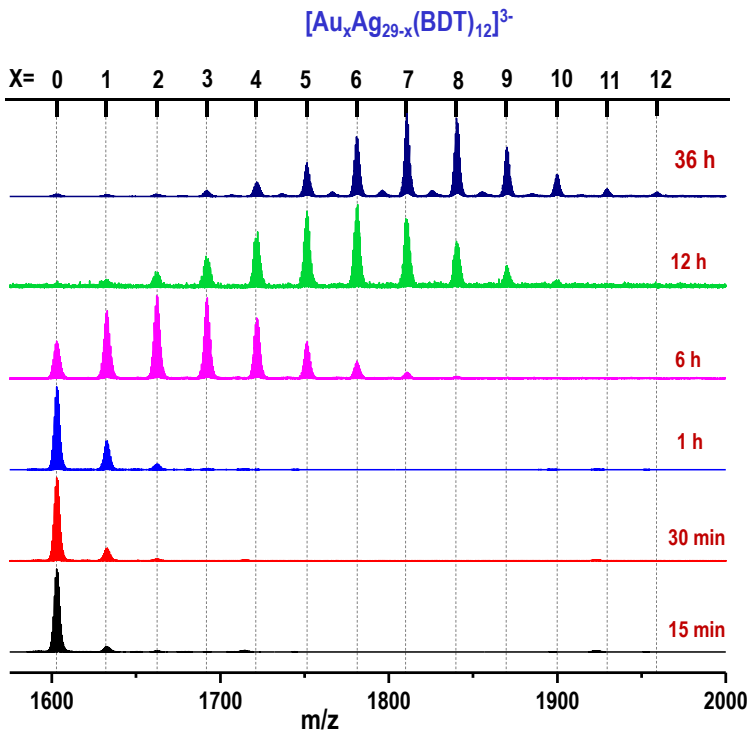

Figure S17. Time-dependent absorption spectra of the reaction between Ag_{29} and Au_{25} (1:5 ratio) at room temperature resulting in the formation of Au_xAg_{29-x} (x = 1-12).

Supporting information 18:

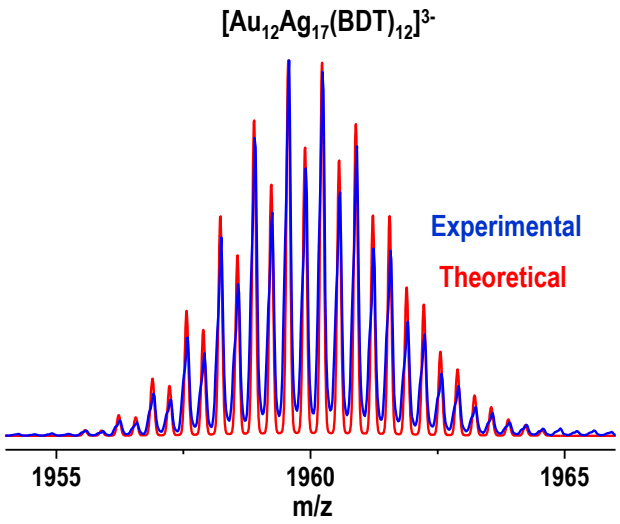

Figure S18. Experimental and theoretical isotopic patterns of $Au_{12}Ag_{17}$ which shows good agreement with each other.

Supporting information 19:

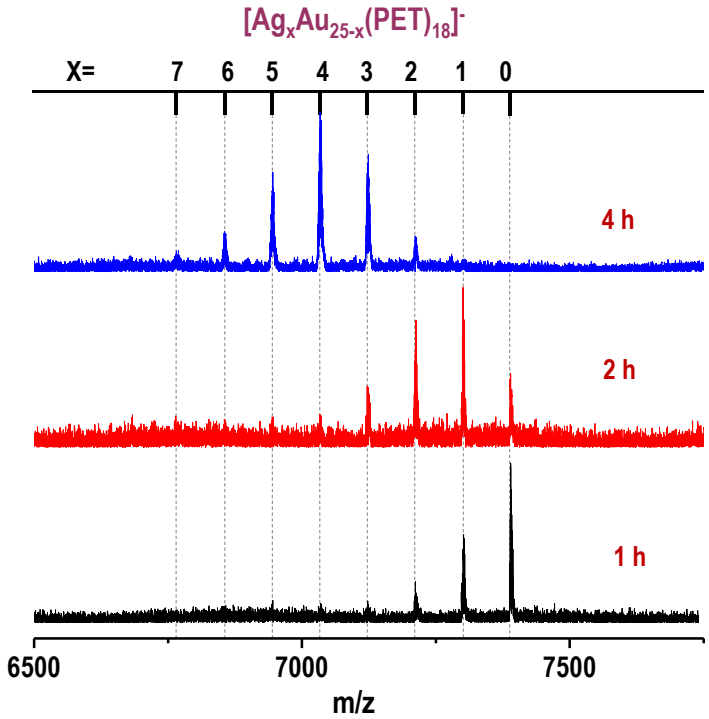

Figure S19. Time-dependent ESI MS of the reaction between Ag_{29} and Au_{25} (1:5 ratio) at the Au_{25} side (higher temperature).

Supporting information 20:

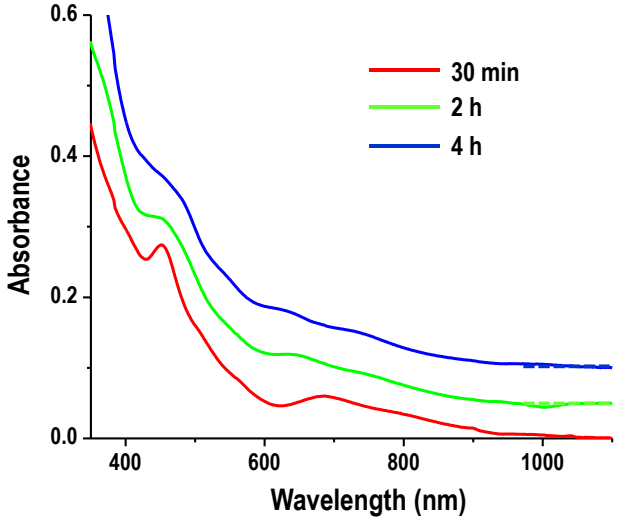

Figure S20. Time-dependent UV-vis absorption spectra of the intercluster reaction between Ag_{29} and Au_{25} using a 1:5 molar ratio.

Supporting information 21:

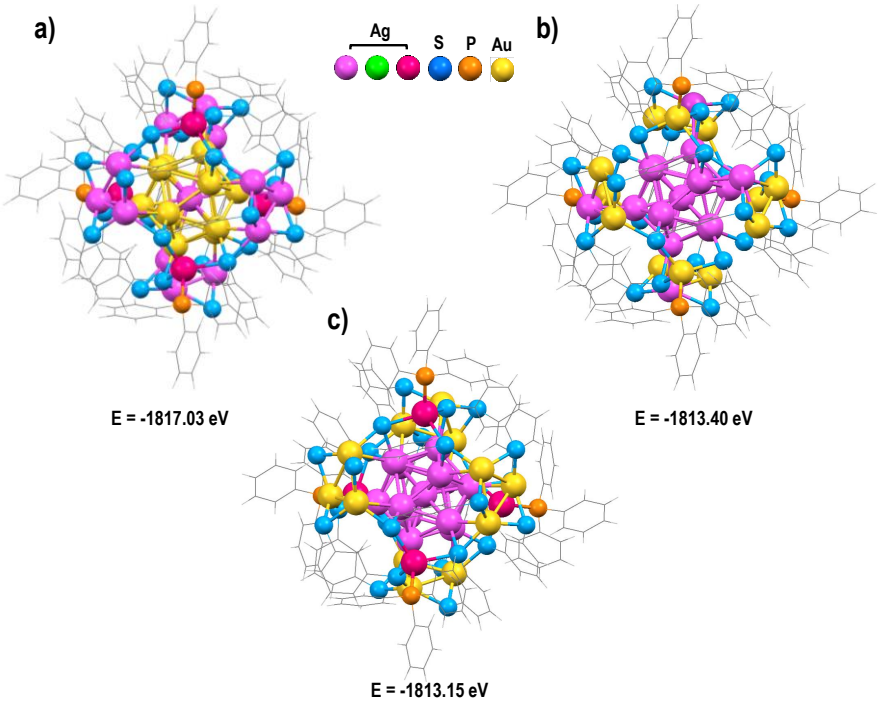

Figure S21. Three different geometric isomers of $Au_{12}Ag_{17}$; (a) 12 Au atoms are doped in the icosahedral surface, (b) among 12 Au atoms, 8 Au atoms are doped in the crown staples and remaining 4 Au atoms are doped in Ag-PPh_3 motifs and (c) 12 Au atoms are doped in the crown motifs.